Excited State Properties of 7-Hydroxy-4-methylcoumarin in the Gas Phase and in Solution. A Theoretical Study

I. Georgieva and N. Trendafilova*

Institute of General and Inorganic Chemistry, Bulgarian Academy of Sciences, Sofia, Bulgaria

A. Aquino and H. Lischka*

Institute for Theoretical Chemistry, Währingerstrasse 17, University of Vienna, A-1090 Vienna, Austria

Received: May 9, 2005; In Final Form: October 19, 2005

TDDFT/B3LYP and RI-CC2 calculations with different basis sets have been performed for vertical and adiabatic excitations and emission properties of the lowest singlet states for the neutral (enol and keto), protonated and deprotonated forms of 7-hydroxy-4-methylcoumarin (7H4MC) in the gas phase and in solution. The effect of 7H4MC−solvent (water) interactions on the lowest excited and fluorescence states were computed using the Polarizable Continuum Method (PCM), 7H4MC−water clusters and a combination of both approaches. The calculations revealed that in aqueous solution the $\pi\pi^*$ energy is the lowest one for excitation and fluorescence transitions of all forms of 7H4MC studied. The calculated excitation and fluorescence energies in aqueous solution are in good agreement with experiment. It was found that, depending on the polarity of the medium, the solvent shifts vary, leading to a change in the character of the lowest excitation and fluorescence transition. The dipole-moment and electron-density changes of the excited states relative to the ground state correlate with the solvation effect on the singlet excited states and on transition energies, respectively. The calculations show that, in contrast to the ground state, the keto form has a lower energy in the $\pi\pi^*$ state as compared to enol, demonstrating from this point of view the energetic possibility of proton transfer from the enol to the keto form in the excited state.

I. Introduction

Coumarins represent a class of heterocyclic compounds with ring oxygen next to the carbonyl group. These compounds possess remarkable photophysical properties, which find applications in diverse areas. First, the strong absorption cross sections and large radiative yields of coumarins make them suitable for use as laser dyes (at the near-ultraviolet to the green wavelengths), colorants, nonlinear optical chromophores and as excellent probes to study the solvation dynamics in homogeneous solutions and organized media.[1−8] Second, coumarins, in particular the hydroxycoumarins (HCs), are well-known natural products,[9] which have been described as enzyme inhibitors, agents with anticoagulant,[10,11] spasmolytic[12] and anticancer activity,[13,14] sun-screening additives[15] and pesticides.[16]

Due to the importance of 7-hydroxycoumarin and 7-hydroxy-4-methylcoumarin (7H4MC, Figure 1) for photochemistry and photobiology, they have been widely investigated from both experimental and theoretical viewpoints.[17−32] 7HCs possess amphoterous properties, and therefore, proton transfer from the hydroxyl group to the carbonyl oxygen acceptor can occur.[18−22]

The absorption and emission properties of 7HCs in various conditions have been studied experimentally; however, the controversial interpretations of the experimental data demonstrate the complex photophysical behavior of these compounds. Theoretical investigations of the excited state properties of 7HCs have been performed using semiempirical approaches. However, the reliability of these methods to vertical and adiabatic excitations has not been checked so far. For example, the assignment of the first low intensity absorption band of 7HCs (at ∼370 nm) is suspicious. Assuming that 7HCs are partly ionized even in the presence of small amounts of water, some authors suggested that the band is due to a $\pi \rightarrow \pi^*$ transition of the ionic form.[20,21,24] At the same time, other authors predicted that it is a $n \rightarrow \pi^*$ transition of neutral 7HCs in agreement with semiempirical calculations (INDO, CNDO/S-CI, ZINDO-CI/S).[23,25] Obviously, the accurate interpretation of the experimental absorption spectra requires reliable quantum mechanical computations of vertical and adiabatic excitations of neutral, deprotonated and protonated form of 7HCs.

In addition, it is very important to perform theoretical studies considering the solvent effect because the spectroscopic data available have been obtained in solution. Moreover, the experimental radiative lifetime indicated that the character of the lowest singlet emitting state of 7HCs depends on the polarity of the media: it is of $n\pi^*$ character in nonpolar solvents (long lifetime and forbidden emitting transition) and of $\pi\pi^*$ character in polar solvents (short lifetime and allowed emitting transition).[31] Hence, we can expect large effects of the polar solvent on $^1(n\pi^*)$ and $^1(\pi\pi^*)$ states. Up to now an explanation of the different character of the excited and emitting states of 7H4MC in nonpolar (which approaches gas phase) and polar solvents has not been given. The investigation of the media effect on the character of the excited and emitting states of 7HCs is important for their application as laser.

The absorption spectra of 7HCs indicated three forms in the electronic ground state depending on the solvent and pH:[20,21] neutral (enol, **E**), protonated (cation, **C**) and deprotonated (anion,

* Corresponding authors. E-mail: N.T., ntrend@svr.igic.bas.bg; H.L., hans.lischka@univie.ac.at.

10.1021/jp0524025 CCC: $30.25
Published on Web 12/06/2005

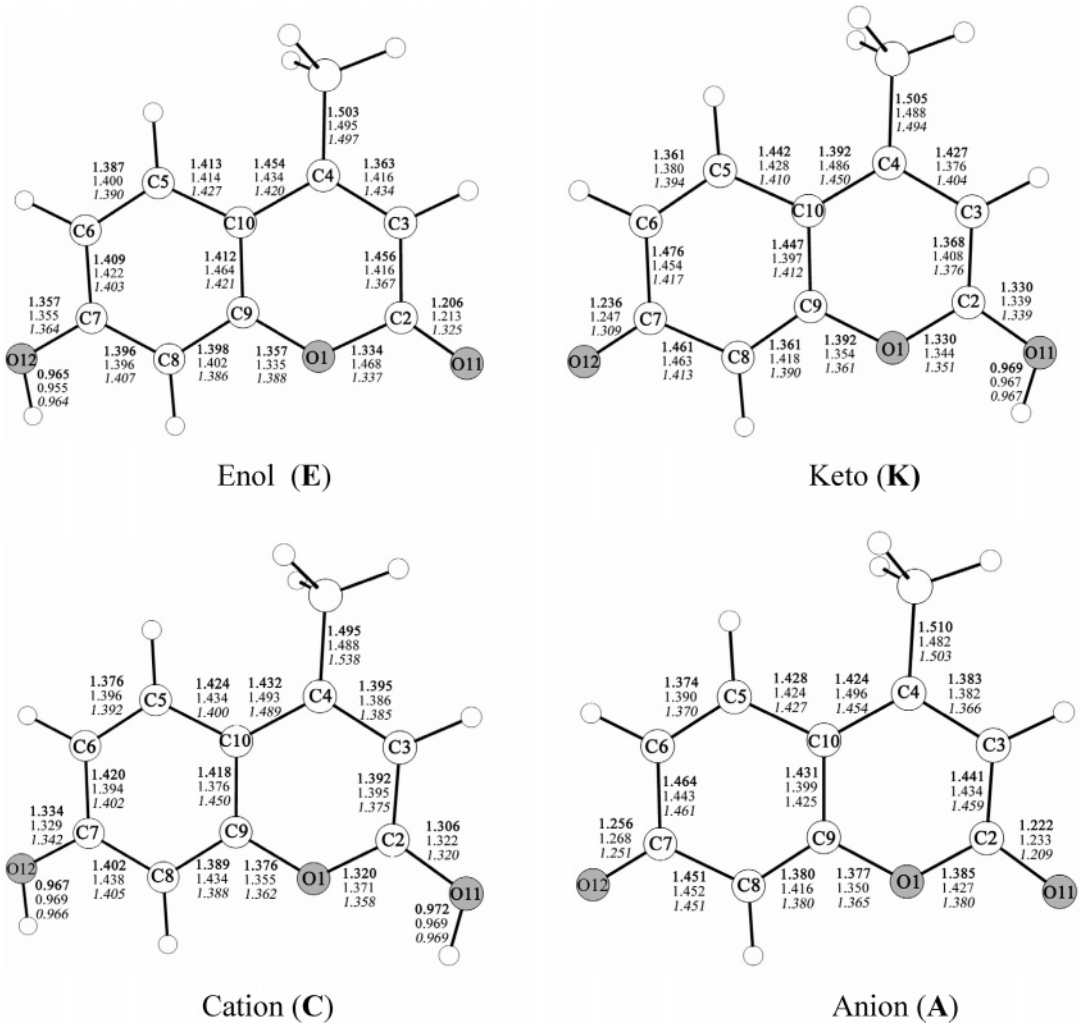

Figure 1. **E**, **K**, **C** and **A** forms of 7H4MC with atom numbering and selected optimized bond lengths in the ground state (**bold**), in the $^1A'(\pi\pi^*)$ state (normal), and in $^1A''(n\pi^*)$ state (for $A-\pi\sigma^*$) (*italic*) at the B3LYP/SVPD level.

A). At the same time, fluorescence spectra showed four species in the excited state: neutral (enol, **E***), anion (**A***), cation (**C***) and a long-wavelength emitting ketotautomeric form (**K***). The **K** form is an excited state reaction product, which arises from the enol **E*** form. Hence, it is expected that in the excited state tautomerization of 7HCs through the proton transfer between the acidic (OH) and basic (C═O) groups proceeds.

The explanation of photochemical and photophysical properties of 7HCs requires detailed study of vertical and adiabatic excitation and fluorescence processes of the compounds studied using appropriate theoretical approaches. Such investigations have been done for 7-amino-4-methylcoumarin with the complete active space self-consistent field (CASSCF) and complete active space perturbation theory to second order.[33] However, the required computer time for such calculations is very large. Therefore, conceptually simpler and more economic methods such as density functional theory (DFT) are required for investigations of the excited state of large molecules. The time-dependent (TD) DFT version using hybrid functionals has been applied successfully for excited state calculations, e.g., in the investigations on a series of 7-aminocoumarin derivatives[33] and also for the study of excited state proton transfer processes.[34,35]

Major methodological progress has been achieved by the variational formulation of the TDDFT method by Furche and Ahlrichs facilitating the calculation of analytic TDDFT gradients, thus allowing geometry optimizations in excited states.[36] So far, much more experience concerning the applicability of DFT is available for the electronic ground state than for the excited states. In our previous paper, the adequacy of DFT/B3LYP level of theory to reproduce the geometry parameters of 7H4MC was verified and this method was successfully applied to the ground state property investigations.[37] The present work is focused on the application of TDDFT/B3LYP to study the excited state properties of 7H4MC. We decided to employ as an additional method the approximate coupled cluster singles and doubles method (CC2)[38] to assess the reliability of the TDDFT/B3LYP results. In combination with the resolution of the identity (RI) procedure[39] CC2 is a computationally very efficient approach incorporating dynamical electron correlation effects. The recent introduction of linear response theory (LRT) in combination with analytic gradients[40] provides the required possibilities for treatment of excited states.

The study of excited state properties in condensed phases is complicated because simulation of the environment is required. An approach based on reaction-field methods considers the solvent as a homogeneous continuum.[41,42] In general, such a bulk interaction solvent model can reproduce solvation effects well. However, in some cases (e.g., when specific solute−solvent interactions are involved) it is necessary to include explicit solvent molecules reproducing part of the first solvation shell. Additionally, long-range interactions with the bulk of the solvent are recovered by embedding the cluster in a continuum.

The aim of the present work is to calculate the vertical and adiabatic excitations and emission properties of the lowest

singlet states in the gas phase and in solution for enol, keto, cationic and anionic species of 7H4MC. The effect of 7H4MC−water interaction on the lowest excited state is estimated using a bulk interaction solvent model as well as a cluster model. The theoretical results obtained are used to provide a well-founded interpretation of the experimental observations and to refine explicitly the ambiguous discussions in the literature. Geometry parameters, electron density and thermodynamical data for the ground and excited states in the gas phase and in solution are obtained and are used to explain the photochemical behavior of the 7H4MC species. As a first step into the proton transfer study of 7H4MC, an energy diagram is given containing the energies of the stationary points and of Franck−Condon structures. The future goal of our investigations will be modeling of proton transfer reaction for 7H4MC in excited state through bridging water molecules.

II. Computational Details

The TURBOMOLE program package[43] has been used for the TDDFT[36,44,45] and RI-CC2[39,40] calculations. The B3LYP[46] functional was chosen for TDDFT calculations of the 7H4MC species. Geometry optimizations of the 7H4MC species in the ground and excited states ($^1\pi\pi^*$ and $^1n\pi^*$) have been performed using the following basis sets: SVP (split valence plus polarization),[47] SVPD (+diffuse functions),[47] TZVP (triple-ζ valence plus polarization)[48] and TZVPD (+diffuse functions).[48] Diffuse functions (one s and one p set) for the C and O atoms as well as for the H atoms were added to the standard SVP and TZVP basis sets to improve the description of negatively charged molecular regions. The exponents of these additional basis functions were obtained by dividing the smallest respective exponent of the SVP and TZVP basis sets by a factor of 3. The final contracted basis set of SVPD is [4s3p1d] for O and C, and [3s2p] for the H atom. The contracted TZVPD basis set is [6s4p1d] for O and C, and [4s2p] for the H atom. To assess the quality of the TDDFT results, the coupled-cluster singles-and-doubles model (CC2) with the SVPD basis set was applied. The resolution-of-the-identity (RI) approximation used in the RI-CC2 calculations is described in ref 49. The ground state minima on the potential energy surfaces, calculated at B3LYP/SVPD level were qualified by the absence of imaginary normal-mode frequencies. Electron density differences between ground and excited states of 7H4MC species have been computed with the CIS method using the SVPD basis set. The standard model ideal gas, rigid rotator and harmonic oscillator is used for enthalpies and Gibbs free energies of enol and keto forms.

Solvent effects on the ground state properties of 7H4MC optimized structures in solution were examined using the polarizable continuum model (PCM) of Tomasi.[50−52] Solvent effects of excited states were computed at the reaction-field level by the PCM approach, using the most recent version implemented in the GAUSSIAN package[53] and fully described in ref 54. The solvent effect on excited state properties of 7H4MC forms (**E**, **K**, **C** and **A**) were estimated for the optimized ground state structures and the solvent effect on emitting properties were calculated for optimized excited state structures. The ground and excited state optimizations were performed with TURBOMOLE using the B3LYP/SVPD level.

Relative lifetimes have been computed for spontaneous emission using the Einstein transition probabilities according to the formula (in a.u.).[55]

$$\tau = \frac{c^3}{2(\Delta E)^2 f} \qquad (1)$$

TABLE 1: TDDFT and RI-CC2 Vertical Excitation Energies, in eV, for the Lowest Singlet Excited States of the E, K, C and A Forms of 7H4MC

		B3LYP				RI-CC2
geometry	state	SVP	SVPD	TZVP	TZVPD	SVPD
		Enol (**E**)				
gr st (C_s)	$2^1A'$ ($\pi\pi^*$)	4.18	4.13	4.17	4.15	4.27
gr st (C_s)	$1^1A''$ ($n\pi^*$)	4.55	4.56	4.61	4.60	4.77
		Keto (**K**)				
gr st (C_s)	$2^1A'$ ($\pi\pi^*$)	3.11	3.06	3.13	3.11	3.06
gr st (C_s)	$1^1A''$ ($n\pi^*$)	2.81	2.86	2.90	2.89	2.82
		Cation (**C**)				
gr st (C_s)	$2^1A'$ ($\pi\pi^*$)	3.65	3.61	3.65	3.64	3.63
gr st (C_s)	$1^1A''$ ($n\pi^*$)	6.15	6.10	6.17	6.16	6.54
		Anion (**A**)				
gr st (C_s)	$2^1A'$ ($\pi\pi^*$)	3.29	3.19	3.27	3.20	3.12
gr st (C_s)	$^1A''$ ($n\pi^*$)[a]	3.39 (1)	3.44 (2)	3.48 (1)	3.47 (2)	3.49 (2)
gr st (C_s)	$^1A''$ ($\pi\sigma^*$)[a]	4.82 (4)	3.08 (1)	4.37 (2)	2.97 (1)	3.19 (1)

[a] The $^1A''$ state numbering of the anionic form is given in parentheses.

where c is the velocity of light, ΔE is the transition energy, and f is the oscillator strength.

III. Results and Discussion

III.A. Basis Set Dependence of Vertical Excitation Energies. To select an efficient basis set, which reliably describes the vertical electronic excitation energies at the equilibrium geometry of the 7H4MC species, the excitation energies were calculated with the SVP, SVPD, TZVP and TZVPD basis sets. All calculations were performed for C_s symmetry of the **E**, **K**, **C** and **A** forms of 7H4MC. The ground state structures of the species studied and atom numbering are presented in Figure 1. The vertical excitation energies of the lowest $^1A'$ and $^1A''$ states, calculated at the TDDFT and RI-CC2 levels are collected in Table 1.

The extension of the basis set from SVP to TZVP leads to a small decrease in the excitation energy (~0.02 eV) for the $\pi \rightarrow \pi^*$ transition and an increase of the excitation energy (up to 0.09 eV) for the $n \rightarrow \pi^*$ transition (compare SVP and TZVP calculations, Table 1). The inclusion of diffuse functions produces a decrease of the $^1(\pi\pi^*)$ excitation energies of ~0.05 eV for the neutral and cationic systems and of ~0.1 eV for the anionic form. A more drastic effect of the diffuse functions is observed for the anion. A $\pi\sigma^*$ state is stabilized significantly, and as a result, the lowest $^1A''$ state is of $\pi\sigma^*$ character. The reason for this strong basis set dependence in this case is the diffuse (Rydberg-type) character of the σ^* orbital. Thus, it can be concluded that the $^1(\pi\pi^*)$ excitation energies depend weakly on the addition of the polarization functions and decrease slightly with addition of diffuse functions. The energy and character of the lowest $^1A''$ state of 7H4MC species appeared to be more sensitive to both polarization and diffuse functions. Furthermore, we will show that the large $n\pi^*$ energy variation is not accidental because the $n \rightarrow \pi^*$ transition of the **E**, **K**, **A** forms is localized on the C═O bond (C−O for **A**), which is sensitive to the basis set used. Using different basis sets, the smallest variations of excitation energies were found for the **C** form and the largest changes for the **A** form. The latter result showed that inclusion of diffuse functions for the anionic species is of great importance for accurate excited state calculations. Despite the variations observed, all TDDFT/B3LYP calculations showed the same trends: (1) a lower $^1(\pi\pi^*)$ excitation energy in comparison to the $^1(n\pi^*)$ one for the **E** and **C** forms and a lower $^1(n\pi^*)$ excitation energy in relation to the $^1(\pi\pi^*)$ excitation for

the **K** form; (2) the vertical $^1(\pi\pi^*)$ excitation energy decreases in the order **E** > **C** > **A** > **K**, whereas the $^1(n\pi^*)$ one decreases in another order **C** > **E** > **A** > **K**. One exception was only found for the **A** form. The SVP and TZVP transition energy order, $^1A'(\pi\pi^*) < {}^1A''(n\pi^*)$ reverses when the diffuse functions are included (SVPD, TZVPD) because of a significant lowering of the $^1A''(\pi\sigma^*)$ excitation energy, Table 1. It should be mentioned that after protonation of 7H4MC (**C** form) the $n\pi^*$ excitation energy increases dramatically (~2 eV), Table 1. Inspection of the molecular orbital energies suggested strong stabilization of the "n" orbital, which explains the increase of $n\pi^*$ excitation energy. A similar protonation effect has already been observed for formaldehyde.[56]

The comparison of the TDDFT and RI-CC2 results in Table 1 shows that there is quite generally good agreement between the results obtained with the two methods. One exception is the $n\pi^*$ state of the cation where a discrepancy of 0.4 eV is observed. This state is very high in energy and not of primary interest in this investigation. On the basis of the observed agreement between RI-CC2 and TDDFT results, we continued with the latter method, which is computationally much more efficient. The results reveal that diffuse functions are important, especially for the description of the anionic form and that the SVPD basis set should be a good compromise. Therefore, all subsequent calculations were performed with SVPD basis set.

It is important to emphasize that as opposed to semiempirical results for 7HC (INDO method)[23] and for 7H4MC (CNDO/S-CI and ZINDO methods),[25] both TDDFT and CC2 methods indicated a $\pi\pi^*$ character of the lowest singlet excitation of **E** tautomer. Thus, we conclude that the suggested $n\pi^*$ character by semiempirical methods as the lowest vertical excitation is not correct.

III.B. Structural and Electronic Characteristic of 7H4MC Forms. In the first step, all geometries have been optimized at the B3LYP/SVPD level using C_s symmetry. The optimized bond distances in the ground and the lowest $^1A'(\pi\pi^*)$ and $^1A''$ states are presented in Figure 1. For all structures a normal-mode analysis has been performed. For the $^1(\pi\pi^*)$ states and the $^1(\pi\sigma^*)$ state of the anion the SVPD basis has been used. For the remaining $^1(n\pi^*)$ states we chose the less time-consuming SVP basis. The **C** and **A** structures for the $^1(\pi\pi^*)$ state are minima in C_s symmetry. One imaginary frequency (-54 cm^{-1}) was found for **E** in the $^1(\pi\pi^*)$ state owing to an out-of-plane mode including the ring O1 atom, Figure 1. Following this mode, the enol geometry was re-optimized in C_1 symmetry. The calculated energy difference of C_1 and C_s structures is very small (~0.01 eV). Two imaginary frequencies were obtained for the $^1(\pi\pi^*)$ state of the **K** structure. However, it should be mentioned that a SVP calculation shows the $^1(\pi\pi^*)$ state of **K** to be a minimum in C_s symmetry. Optimization of the $^1(\pi\pi^*)$ **K** structure in C_1 symmetry failed because of persistent state-switching between $^1(\pi\pi^*)$ and $^1(n\pi^*)$ states. The optimized **E** and **K** structures in the $^1(n\pi^*)$ state as well as the **A** structures in $^1(n\pi^*)$ and $^1(\pi\sigma^*)$ states are found to be minima in C_s symmetry. Only the **C** structure in the $^1(n\pi^*)$ state shows one imaginary frequency in C_s symmetry owing to ring torsion. The further attempt to optimize the geometry of the $^1(n\pi^*)$ state of the **C** form in C_1 symmetry failed for similar state-switching reasons as in the keto case described above. We had already noted above that this state is not of big interest to us because of its relatively large excitation energy. In conclusion of our geometry optimization efforts we note that most of the structures were minima at C_s symmetry or, as in the case of the $^1(\pi\pi^*)$ state of **E**, the reduction to C_1 symmetry had negligible effects. In case of the $^1(\pi\pi^*)$ state of the keto structure the C_1 geometry optimization failed. However, because the smaller SVP basis showed no imaginary frequencies, we expect also here that geometry relaxation effects in C_1 geometry will not be significant. Therefore, we continued in our further investigation with C_s symmetry restriction, which allowed a clear distinction of $\pi\pi^*$ and $n\pi^*$ states, avoiding interactions between states the TDDFT method is not designed for. Full Cartesian geometries are given in the Supporting Information (see the end of the text for more information).

Large bond length variations were calculated for the **E**, **K**, **C** and **A** forms in the ground and in the excited states indicating strong and specific electron conjugation in the coumarin fragment of the species studied (see Figure 1). In the ground state the protonation of the **E** form leads to elongation of the C2−O11, C9−O1 and C6−C7 bond lengths and to shortening of the C2−C3, C2−O1 and C7−O12 bond lengths. On the other side, the deprotonation of the C7O12H group produces a shortening of the C7−O12 and C8−C9 bond lengths and an elongation of the C6−C7, C7−C8, C9−O1, C2−O1 and C2−O11 bond lengths. As discussed in ref 37, assuming bond polarizations of **A** form as basic ones, the bond length changes in the **E**, **K** and **C** forms could be explained by the direction of induced polarization produced by H atom binding.

Different bond-length changes were obtained going from ground to $^1(\pi\pi^*)$ and $^1(n\pi^*)$ excited states. In general, the $\pi \rightarrow \pi^*$ transitions affect the π-density of the coumarin ring bonds. As it is seen from Figure 1, for the **K**, **C** and **A** forms in the $^1(\pi\pi^*)$ excited state the C8−C9, C10−C4, C2−C3 and C5−C6 bond lengths increase and the C9−C10, C6−C7, C9−O1 and C3−C4 bond lengths decrease. At the same time, for the $\pi\pi^*$ excited state of the **E** form, the C9−C10, C3−C4, C4−C10 and C6−C7 bond lengths change in reverse directions. The calculated electron density differences between the ground and the excited states for **E**, **K**, **C** and **A** species show the same trends: the excitation to the $\pi\pi^*$ excited state pushes the electron density to the C4 and C2 atoms, while electron density on the C10 and C3 atoms decreases (see Figure 2). Hence, the observed electron density changes indicate charge transfer character of the $\pi \rightarrow \pi^*$ transition but do not explain the bond length changes in the forms studied. Better understanding of the effect of the electronic excitation on the bond length changes could be obtained analyzing the HOMO (π) and LUMO (π^*) represented in Figure 3. Considering LUMO with relation to HOMO of the **E** form, the bonding character along the C9−C10, C6−C7 and C4−C3 bonds is decreased, while the π-density on C10−C4 and C3−C2 bonds is increased. As a consequence, an elongation of the C9−C10, C6−C7 and C4−C3 bonds (+0.052 Å, +0.013 Å, +0.053 Å) and a shortening of the C10−C4 and C3−C2 bonds (−0.02 Å, −0.04 Å, respectively) was obtained. The **K**, **C**, and **A** forms have different HOMO (π) and LUMO (π^*) characters, which explain the corresponding bond length changes by $\pi \rightarrow \pi^*$ transition, Figure 3a−c in Supporting Information. The $n \rightarrow \pi^*$ transition affects the carbonyl group (C7−O12) in the **E** and **K** structures in agreement with the character of the HOMO−2 (n) orbital, Figure 3. Due to the $n \rightarrow \pi^*$ transition there is an in-plane electron depletion around the carbonyl oxygen (Figure 2) that produces substantial increase of the C═O bond lengths for **E*** and **K*** (see Figure 1). For the **C** form the lone pair orbitals are stabilized due to protonation and electron density changes for $n\pi^*$ excitation are in the C4−C(H_3) region, leading to an elongation of the C4−C(H_3) bond.

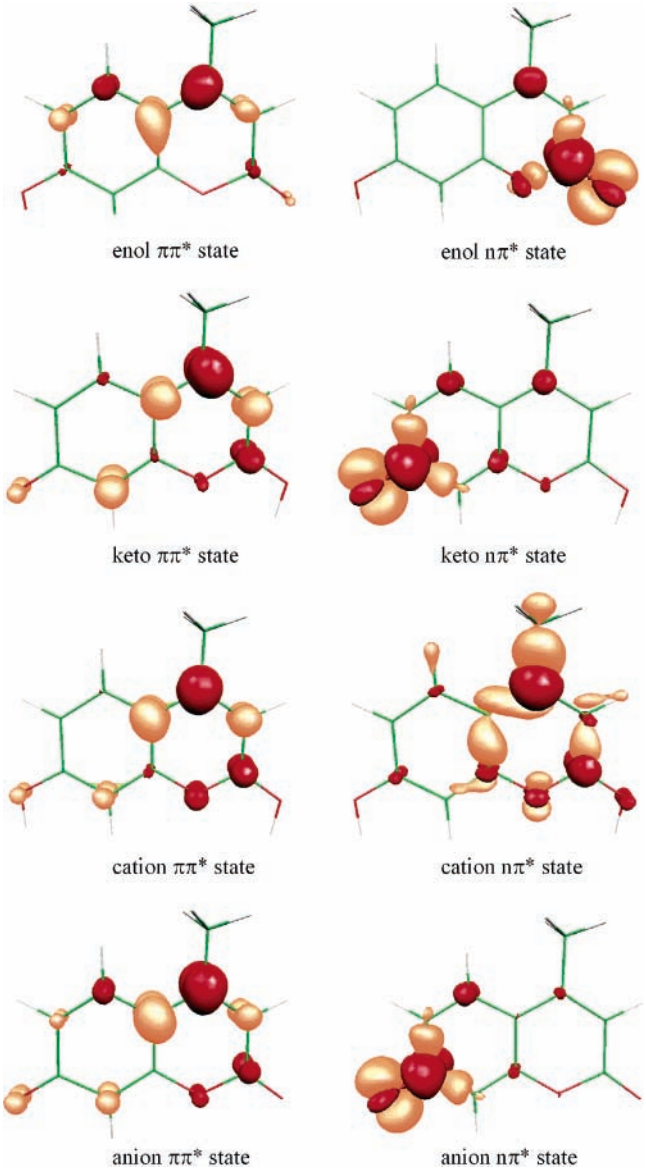

Figure 2. Electron density differences for the $\pi\pi^*$ and $n\pi^*$ excited states relative to the ground state of enol, keto, cationic and anionic form of 7H4MC, calculated with the CIS method. The black region indicates an increase of the electron density and the grey regions a decrease of the electron density.

III.C. Vertical Excitation Energies of 7H4MC Species in Aqueous Solution. First, the solvent effect was estimated on the basis of the PCM model. To check the reliability of the continuum model, 7H4MC−water cluster models were considered, taking into account the specific solute−solvent interactions. Further, a semicontinuum model was applied to 7H4MC−water clusters. TDDFT/B3LYP/SVPD vertical excitation energies of the lowest singlet states of the **E**, **K**, **C** and **A** forms as well as of cluster structures of **E** and **K** with two and four water molecules are given in Table 2 for the gas phase and for aqueous solution.

We start our analysis with a discussion of solvation effects for the $^1(\pi\pi^*)$ and $^1(n\pi^*)$ states of the **E** and **K** structures. The enol geometry has been optimized at the B3LYP/SVPD level in the gas phase, in aqueous solution with the PCM model and for two cluster models composed by (1) enol and two water molecules bound to the carbonyl oxygen and the hydroxyl hydrogen; (2) enol and four water molecules, where two of them are bound to the carbonyl oxygen and two to the hydroxyl group

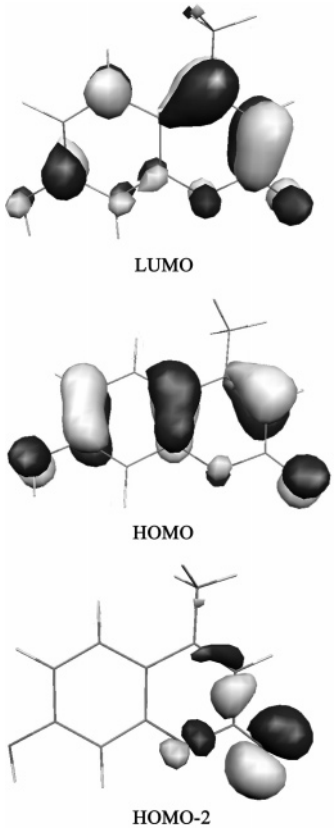

Figure 3. LUMO (π^*), HOMO (π), and HOMO−2 (n) of the E form.

as shown in Figure 4. The enol-$(H_2O)_2$ cluster was optimized in C_s and C_1 symmetry for the ground and $^1(\pi\pi^*)$ excited states and stabilization of C_1 symmetry was obtained by 0.5 and 0.47 kcal/mol, respectively. The calculated transition energies on the basis of the ground and excited state structures in C_1 and C_s symmetry, however, give practically the same values. For that reason the excited state properties of the cluster models were examined using C_s symmetry structures only, which facilitated calculations and assignments considerably. The Cartesian coordinates of the optimized structures of the water clusters of **E** and **K** forms are given in the Supporting Information.

The main solvent effect on the geometrical parameters of **E** in the ground state is the elongation of the C2═O11, O1−C2 and O12−H bonds and the shortening of the C7−O12(H) bond (Table 3). A similar elongation of a C═O double bond because of solvation effects has been observed, e.g., by Andrade do Monte et al. for formaldehyde.[57]

The calculated excited state electron density of the **E** form in aqueous solution (PCM) relative to the ground state density indicated that the electron density increases on the carbonyl oxygen, whereas it decreases on the hydroxyl hydrogen. The solvent polarization effect produces an additional polarization of the C═O bond by which the electron density on O atom increases and as a result the C═O bond become longer. The solvent effect on the enol geometry in enol-$(H_2O)_4$ and in the continuum model are in good agreement, whereas in the enol-$(H_2O)_2$ cluster model it is smaller, Table 3.

In general, a bathochromic solvent shift is calculated for the $^1(\pi\pi^*)$ excitation energy and a hypsochromic solvent shift is found for the $^1(n\pi^*)$ one of **E** (see Table 2). The gas phase $^1(\pi\pi^*)$ excitation energy (4.13 eV) is higher than the experimental one in aqueous solution by 0.27 eV. The calculated PCM solvent shift decreases the $^1(\pi\pi^*)$ excitation energy and brings it into better agreement with experimental. Both enol-$(H_2O)_2$

TABLE 2: TDDFT/B3LYP Vertical Excitation Energies, in eV, for the Lowest Singlet States of the E, K, C and A Forms of 7H4MC in the Gas Phase and in Aqueous Solution (PCM) Using the SVPD Basis Set

geometry	state	gas phase[a]	gas phase[b]	aq soln[c]	exp[20,21] aq soln
		Enol (**E**)			
gr st (C_s)	$2^1A'$ ($\pi\pi^*$)	4.13 (0.28)[d]	4.09	3.97	3.86
gr st (C_s)	$3^1A'$ ($\pi\pi^*$)	4.52		4.40	
gr st (C_s)	$1^1A''$ (nπ^*)	4.56	4.37	4.83	
gr st (C_s)	$2^1A''$ ($\pi\sigma^*$)	5.32	5.06	5.46	
		Enol-$(H_2O)_2$			
gr st (C_s)	$2^1A'$ ($\pi\pi^*$)	4.05 (0.34)	4.00	3.90	
gr st (C_s)	$3^1A'$ ($\pi\pi^*$)	4.46		4.36	
gr st (C_s)	$1^1A''$ ($\pi\sigma^*$)	4.62	4.53	5.43	
gr st (C_s)	$2^1A''$ (nπ^*)	4.80	4.54	5.04	
		Enol-$(H_2O)_4$			
gr st (C_s)	$2^1A'$ ($\pi\pi^*$)	4.05 (0.35)			
gr st (C_s)	$3^1A'$ ($\pi\pi^*$)	4.42			
gr st (C_s)	$1^1A''$ ($\pi\sigma^*$)	4.89			
gr st (C_s)	$2^1A''$ (nπ^*)	4.98			
		Keto (**K**)			
gr st (C_s)	$2^1A'$ ($\pi\pi^*$)	3.06 (0.24)	2.91	3.09	
gr st (C_s)	$3^1A'$ ($\pi\pi^*$)	4.19		4.17	
gr st (C_s)	$1^1A''$ (nπ^*)	2.86	2.66	3.48	
		Keto-$(H_2O)_2$			
gr st (C_s)	$2^1A'$ ($\pi\pi^*$)	3.10 (0.28)	2.98	3.13	
gr st (C_s)	$3^1A'$ ($\pi\pi^*$)	4.14		4.17	
gr st (C_s)	$1^1A''$ (nπ^*)	3.20	3.05	3.74	
		Keto-$(H_2O)_4$			
gr st (C_s)	$2^1A'$ ($\pi\pi^*$)	3.09 (0.28)			
gr st (C_s)	$3^1A'$ ($\pi\pi^*$)	4.07			
gr st (C_s)	$1^1A''$ (nπ^*)	3.47			
		Cation (**C**)			
gr st (C_s)	$2^1A'$ ($\pi\pi^*$)	3.61 (0.21)	3.61	3.61	3.59
gr st (C_s)	$3^1A'$ ($\pi\pi^*$)	4.02		4.10	
gr st (C_s)	$1^1A''$ (nπ^*)	6.10	5.78	5.74	
		Anion (**A**)			
gr st (C_s)	$2^1A'$ ($\pi\pi^*$)	3.19 (0.31)	3.14	3.32	3.44
gr st (C_s)	$3^1A'$ ($\pi\pi^*$)	4.10		4.28	
gr st (C_s)	$1^1A''$ ($\pi\sigma^*$)	3.08	3.08	4.51[e]	
gr st (C_s)	$2^1A''$ (nπ^*)	3.44	3.30	3.98[e]	

[a] Gas phase calculation with optimized gas phase structure. [b] Gas phase calculation with optimized ground state PCM structure. [c] PCM calculation with optimized PCM structure. [d] Oscillator strengths (absorption) are given in parentheses for vertical $\pi \rightarrow \pi^*$ transitions. Oscillator strengths for $n \rightarrow \pi^*$ transitions are less than 10^{-3} and are not given in the table. [e] The order of $^1A''$ states of A form in solution is $1^1A''$ (nπ^*), $2^1A''$ ($\pi\sigma^*$).

and enol-$(H_2O)_4$ clusters (third column, Table 2) show negative solvent shifts for the $^1(\pi\pi^*)$ excitation also, but they are smaller in comparison with the PCM results (enol, fifth column) and with experiment, indicating that two or four water molecules are not sufficient to describe the whole solvent effect. On the other side, the pure PCM approach also underestimates the total solvent shift slightly by 0.1 eV as compared to experiment. When we consider the enol-$(H_2O)_2$ cluster embedded in the dielectric continuum, the $^1(\pi\pi^*)$ excitation energy obtained (3.90 eV) is in excellent agreement with experiment (3.86 eV) (Table 2). Obviously, the reliable estimation of solvent shift on the excitation energies requires inclusion of both specific and bulk interactions in the solvation model.

A large hypsochromic solvent effect for the singlet $n \rightarrow \pi^*$ transition was calculated for **E** (0.48 eV) with PCM and with both cluster models. Adding a polarizable continuum to the cluster models, the positive solvent effect increases by 0.2 eV, indicating important long-range interactions with the bulk of the solvent. It is interesting to note that for both cluster models the lowest $^1A''$ excited state is of $\pi\sigma^*$ character in the gas phase and of nπ^* character in aqueous solution.

The same approach for calculating the solvent effect was applied to the **K** form. Although, there is lack of experimental absorption data for **K**, it is interesting to follow the solvent shift for both singlet excited states. Both PCM and cluster models suggested a small hypsochromic solvent shift of the keto $\pi \rightarrow \pi^*$ transition (~0.07 eV). At the same time, as for the **E** form, a very large positive solvent shift was obtained (~0.88 eV) for $n \rightarrow \pi^*$ transition of **K**. Comparing the explicit solvation and semicontinuum models with the direct PCM result given in Table 2, we find that the latter underestimates the overall solvatochromic shift somewhat but still reproduces the solute−solvent interaction quite well.

The solvent shift of the singlet excitation energies of the **C** and the **A** forms was calculated on the basis of the PCM model also (see Table 2). For the **C** form, there was practically no solvent shift observed for the $\pi \rightarrow \pi^*$ transition and a negative one (~0.35 eV) was found for the $n \rightarrow \pi^*$ transition. For the **A** form, positive solvent shifts were calculated for the $^1(\pi\pi^*)$, $^1(\pi\sigma^*)$ and $^1(n\pi^*)$ excitations, 0.1, 1.4, and 0.5 eV, respectively. It should be noted that for the **A** form in the gas phase the $\pi \rightarrow \sigma^*$ transition showed the lowest energy, whereas in aqueous solution the lowest energy transition is $\pi \rightarrow \pi^*$. The analogical trend was found for the **K** form. The calculated excitation energies in aqueous solution for **C** and **A** forms are in good agreement with experiment, Table 2 (fifth and sixth columns), indicating that the PCM model reliably estimates the solvent shift of the excitation energies of the ionic species.

In addition, the vertical excitation energies of $3^1A'$ ($\pi\pi^*$) states in gas phase and solution for the species studied are given in Table 2. For the enol systems and cationic form the $3^1A'$ ($\pi\pi^*$) state appears to be the second singlet excited state.

The calculations reveal that in aqueous solution the $\pi\pi^*$ excitation energy is the lowest one for the **E**, **C** and **A** forms of 7H4MC. In agreement with experiment, the **A** form showed the lowest $\pi\pi^*$ excitation energy from these three compounds, followed by the **C** and by **E**, Table 2 (fifth and sixth columns). Therefore, in the absorption spectra of 7H4MC in aqueous solution, the assignment of the band at ~360 nm (3.44 eV) to the $n \rightarrow \pi^*$ transition of enol 7H4MC (computed at 4.83 eV) is not correct.[23] According to our vertical excitation calculations this band should be assigned to the **A** form of 7H4MC (3.32 eV).

The solvent shift can be split into two contributions: geometry relaxation changes between the gas phase and solution and the polarization induced by the solvent. The geometry relaxation effect is computed by calculating the electronic excitation at the ground state geometries optimized in the gas phase and in solution, without including any other solvent effect (as a difference between the values in 4th and 3rd columns). The solvent polarization effect is found by computing the excitation energy in the gas phase and solution at a fixed geometry (as a difference between the values in fifth and fourth columns). In general, it is observed that for both singlet states the geometry effect reduces the excitation energies (0.04−0.3 eV). The solvent polarization, however, produces various effects on the different excited states and it dominates the total solvent shift. As seen from Table 2, very large positive solvent shifts were obtained for the $^1A''$ states of the **E**, **K** and **A** forms due to the polarization effect. Only for the **C** form the geometry and the polarization effects are negligible.

To get a better understanding of the various solvent shifts for the 7H4MC species, the dipole moments in ground and in

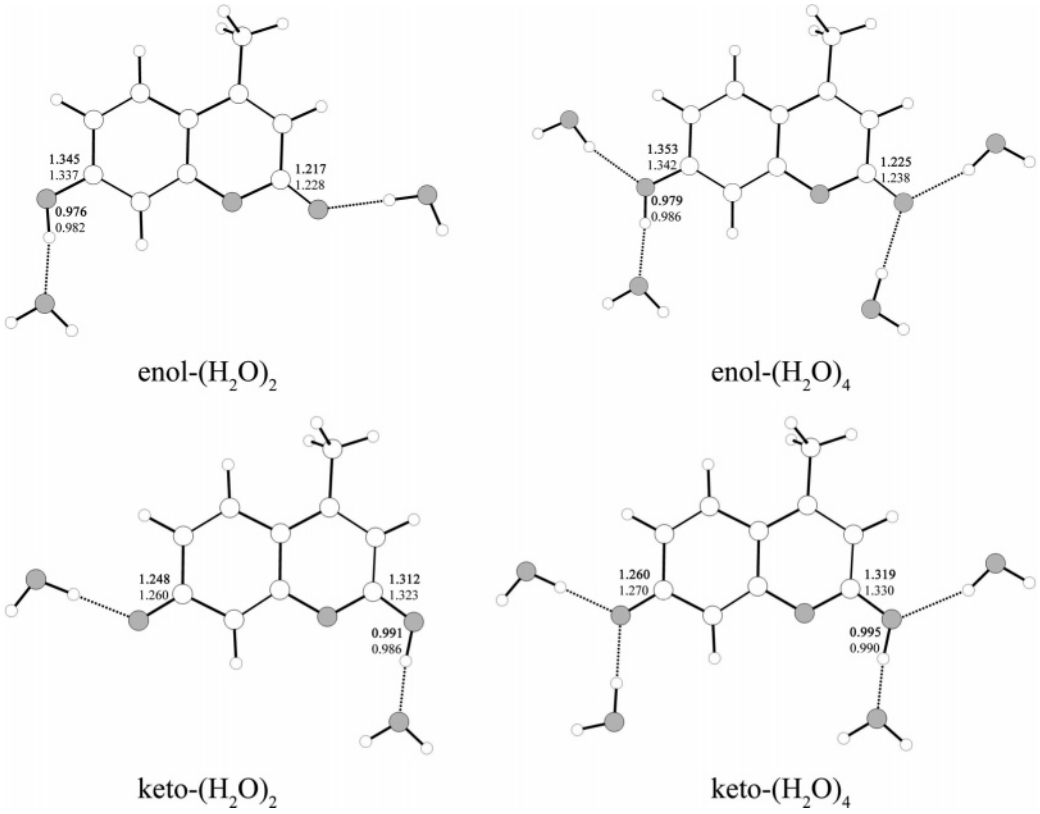

Figure 4. Enol and keto clusters with two and four water molecules optimized at the B3LYP/SVPD level.

TABLE 3: Selected Bond Lengths (Å) of the E and K Forms of 7H4MC in Gas Phase and in Aqueous Solution (PCM) at the B3LYP/SVPD Level

bond[a]	tautomer gas phase	tautomer aq sol	cluster1[b] gas phase	cluster1[b] aq sol	cluster2[c] gas phase
			Enol (**E**)		
C2═O11	1.206	1.222	1.217	1.228	1.225
O1−C2	1.334	1.377	1.379	1.370	1.368
O12−H	0.965	0.987	0.976	0.989	0.979
C7−O12	1.357	1.350	1.345	1.343	1.353
			Keto (**K**)		
C7═O12	1.236	1.263	1.248	1.272	1.260
C7−C8	1.461	1.443	1.452	1.437	1.444
O11−H	0.969	0.999	0.991	1.015	0.995
C2−O11	1.330	1.312	1.312	1.299	1.319

[a] Atom numbering is given in Figure 1. [b] Cluster1: 7H4MC−$(H_2O)_2$. [c] Cluster2: 7H4MC−$(H_2O)_4$.

TABLE 4: Dipole Moment (Debye) for the Ground State and Excited State of the E and K Forms of 7H4MC at the B3LYP/SVPD Level

species	gr st gas phase	gr st aq sol	^{1}A′ ($\pi\pi^*$) gas phase	^{1}A″ (nπ^*) gas phase
E	4.542	7.015	5.322	1.027
K	7.361	13.421	6.648	3.393

singlet-excited states were computed (see Table 4). The dipole moment of E increases when going from the ground to the $^1(\pi\pi^*)$ excited state and at the same time the excitation energy is lowered due to the increased stabilization of the molecule by the polar solvent in the excited state. On the other side, the dipole moment of the $^1(\pi\pi^*)$ excited state of the **K** form decreases and as a result the $^1(\pi\pi^*)$ is destabilized by the solvent relative to the ground state. The strong decrease of the dipole moments of the ^{1}(nπ^*) excited states in the **E** and **K** forms can be related to the positive solvent shift of their ^{1}(nπ^*) excitation energies.

III.D. Vertical Fluorescence Energies of 7H4MC Species in Aqueous Solution. The minimum-to-minimum (m−m) absorption energies and vertical fluorescence energies for **E**, **K**, **C** and **A** forms of 7H4MC were calculated with the TDDFT method using SVP, TZVP and SVPD basis sets (see Table 5a of the Supporting Information). In Table 5 the calculations in the gas phase and in aqueous solution are presented using the SVPD basis set. For all species studied, $\pi\pi^*$ excitation minimum-to-minimum absorption and vertical fluorescence energies slightly decrease with basis set splitting and addition of polarization and diffuse functions (up to 0.05 eV). The zero-point corrections lower the $\pi\pi^*$ absorption energies by 0.03−0.15 eV. The nπ^* energies studied reveal more complex dependence on the basis sets. It is found that with addition of polarization and diffuse functions the nπ^* minimum-to-minimum and fluorescence energies increase for **E**, **K** and **A** (up to 0.1 eV) and decrease for **C** (0.07 eV). The calculated m−m $\pi\pi^*$ transition energies (Table 5) are lower than the vertical ones (Table 2) by 0.19 eV for **A**, 0.2 eV for **E**, 0.25 eV for **C** and 0.36 eV for the **K** form. The values obtained indicate quite large geometry relaxation effects in the $^1(\pi\pi^*)$ state. Geometry relaxation effects on the lowest ^{1}A″ excited state increase in the following order: **A** $^1(\pi\sigma^*)$ ($\Delta = 0.07$ eV), **K** ^{1}(nπ^*) ($\Delta = 0.36$ eV), **C** ^{1}(nπ^*) ($\Delta = 0.4$ eV), **E** ^{1}(nπ^*) ($\Delta = 0.7$ eV) (Δ is the difference between vertical and m−m transition energies).

The TDDFT calculations predict that in the gas state the lowest minimum-to-minimum and the fluorescence transitions for the **E** and **K** forms have nπ^* character, whereas for the **C** form they have $\pi\pi^*$ character. For the **A** form, the SVP and TZVP basis set showed the nπ^* fluorescence energy as the lowest one, whereas TZVPD and SVPD give the $\pi\pi^*$ fluorescence energy as the lowest one, Table 5.

Vertical fluorescence energies of the 7H4MC species were calculated in aqueous solution. Results are compared with the

TABLE 5: TDDFT/B3LYP Minimum-to-Minimum (m−m), Zero-Point Corrected (0−0) Absorption Energies (eV), Vertical Fluorescence Transitions (fl), st Stokes Shift and Radiative Lifetimes[a] of the E, K, C and A Forms of 7H4MC Using the SVPD Basis Set

geometry	state	gas phase	aq sol[b]	exp[20,21,29] aq sol
	Enol (**E**)			
$\pi\pi^*(C_s)$	m−m $2^1A'$ ($\pi\pi^*$)	3.93	3.85	
	0−0 ($\pi\pi^*$)	3.78		
	fl $2^1A'$ ($\pi\pi^*$)	3.73 (6.5)	3.66 (4.5)	3.18 (∼3)
st ($\pi\pi^*$)		0.40	0.31	0.68
$n\pi^*$ (C_s)	m−m $1^1A''$ ($n\pi^*$)	3.86	4.42	
	fl $1^1A''$ ($n\pi^*$)	3.08	3.90	
	Enol-$(H_2O)_2$			
$\pi\pi^*$ (C_s)	fl $2^1A'$ ($\pi\pi^*$)	3.74 (4.8)	3.65 (4.0)	
	Enol-$(H_2O)_4$			
$\pi\pi^*$ (C_s)	fl $2^1A'$ ($\pi\pi^*$)	3.74 (5.1)	3.67 (4.0)	
	Keto (**K**)			
$\pi\pi^*(C_s)$	m−m $2^1A'$ ($\pi\pi^*$)	2.70	2.84	
	0−0 ($\pi\pi^*$)	2.63		
	fl $2^1A'$ ($\pi\pi^*$)	2.28 (38.3)	2.59 (19.1)	2.61 (5.5)
st ($\pi\pi^*$)		0.78	0.50	
$n\pi^*$ (C_s)	m−m $1^1A''$ ($n\pi^*$)	2.50	3.22	
	fl $1^1A''$ ($n\pi^*$)	2.12	3.06	
	Keto-$(H_2O)_2$			
$\pi\pi^*$ (C_s)	fl $2^1A'$ ($\pi\pi^*$)	2.37 (30.4)	2.63 (18.2)	
$n\pi^*$ (C_s)	fl $1^1A''$ ($n\pi^*$)	2.38	3.14	
	Keto-$(H_2O)_4$			
$\pi\pi^*$ (C_s)	fl $2^1A'$ ($\pi\pi^*$)	2.36 (32.9)	2.63 (19.2)	
	Cation (**C**)			
$\pi\pi^*(C_s)$	m−m $2^1A'$ ($\pi\pi^*$)	3.36	3.45	
	0−0 ($\pi\pi^*$)	3.24		
	fl $2^1A'$ ($\pi\pi^*$)	3.02 (37.8)	3.11 (23.1)	2.96
st ($\pi\pi^*$)		0.59	0.50	0.63
$n\pi^*$ (C_s)	m−m $1^1A''$ ($n\pi^*$)	5.70	5.81	
	fl $1^1A''$ ($n\pi^*$)	4.79	4.90	
	Anion (**A**)			
$\pi\pi^*(C_s)$	m−m $2^1A'$ ($\pi\pi^*$)	3.00	3.22	
	0−0 ($\pi\pi^*$)	2.97		
	fl $2^1A'$ ($\pi\pi^*$)	2.74 (16.4)	3.03 (8.8)	2.77 (5.2)
st ($\pi\pi^*$)		0.45	0.29	0.67
$\pi\sigma^*$ (C_s)	m−m $1^1A''$ ($\pi\sigma^*$)	3.01	4.44	
	fl $1^1A''$ ($\pi\sigma^*$)	2.93	4.37	

[a] Radiative lifetimes (ns) for fluorescence are given in parentheses for vertical $\pi \rightarrow \pi^*$ transitions. [b] PCM calculations of optimized excited state structures in gas phase.

experimental fluorescence data, Table 5. For the **E** form, the PCM calculations showed a small negative solvent shift (−0.07 eV) for the $\pi\pi^*$ fluorescence energy and a strong positive solvent effect on the $n\pi^*$ state (+0.82 eV). As a result, in aqueous solution, the lowest fluorescence energy becomes $\pi\pi^*$ (in the gas phase it is $n\pi^*$). To estimate the sensitivity of the lowest fluorescence energy to the solvent polarity, the fluorescence energy was also calculated in the nonpolar solvent cyclohexane. The gas phase and PCM (cyclohexane) calculations showed the same trends, lower $n\pi^*$ fluorescence energy (3.08 eV in gas phase, 3.37 eV in cyclohexane) than $\pi\pi^*$ energy (3.73 eV in gas phase, 3.65 eV in cyclohexane). This finding is in full agreement with experiment, which on the basis of the radiative lifetime predicted a $n\pi^*$ character of the emitting state in nonpolar solvent (71 ns) and $\pi\pi^*$ character in polar solvent (∼3 ns).[31] The radiative lifetime of $\pi\pi^*$ fluorescence (4.5 ns), calculated for aqueous solution of **E** is in better agreement with experiment than the that for gas phase (6.5 ns). Although the negative solvent shift of the calculated fluorescence energy of **E** (3.66 eV) is in the direction to the experimental one in aqueous solution (3.18 eV), it is not sufficient to describe the total solvent shift. Obviously, other solvation relaxation effects contribute to the lowering of fluorescence energy.[58]

As seen from Table 5, large positive solvent shifts were calculated for both $\pi\pi^*$ and $n\pi^*$ fluorescence energies of the **K** form, 0.3 and 0.9 eV, respectively. In contrast to the gas phase, the $\pi\pi^*$ fluorescence energy is the lowest one in polar solution. It is worth emphasizing that due to the positive solvent shift obtained with PCM the calculated fluorescence energy of **K** (2.59 eV) is in very good agreement with experiment in aqueous solution (2.61 eV).

For the **C** and **A** forms the positive solvent shifts of $\pi\pi^*$ fluorescence energies lead into the wrong direction and the computed excitation energies are too large in comparison with experiment (by ∼0.17 eV).

In general, the PCM (water) calculations of vertical fluorescence energies for all 7H4MC species predicted the $\pi\pi^*$ character of the lowest fluorescence transition in agreement with the experiment. At the same time, the calculated $\pi\pi^*$ fluorescence energies decrease in the order: **E** (3.66) < **C** (3.11) < **A** (3.03) < **K** (2.59 eV) in agreement with experiment.[20,21]

III.E. Reactivity of 7H4MC and Its Water Clusters in the Ground and Excited States. The determination of the equilibrium structures of the **E** and **K** forms and their energy difference provides the first ideas of how the molecular frame readjusts during the proton transfer. Figure 5 presents the excitation and fluorescence scheme for 7H4MC. The relative energies of **E** and **K** forms as well as of the corresponding clusters with two and four water molecules are given in Table 6. The electronic, enthalpy and Gibbs energies show that the **E** tautomer is the global minimum in the ground state, whereas the **K** structure is a local minimum structure, which lies 24 kcal/mol above the **E** form. In aqueous solution (PCM and cluster calculations) the relative energy of **K** decreases by 5 kcal/mol. Drastic changes, however, were obtained in the excited state: in the gas phase the relative energy of **E** and **K** forms in the $\pi\pi^*$ excited states (Franck−Condon structures) decreases to 0.35 kcal/mol and in solution the **K** tautomer is even energetically slightly favored. The optimized $^1(\pi\pi)^*$ excited states of both tautomers reveal a lower energy of the **K** form in the gas phase and in aqueous solution. To simulate the optimization of excited states in solution, the tautomer-$(H_2O)_2$ clusters, reproducing a part of the first solvation shell, were optimized and their vertical and adiabatic excited states in solution were calculated. All excited state calculations of clusters suggest a lower energy for the **K** structure as compared to **E** (Table 6). As a result, the **K** form is energetically favored in the $^1(\pi\pi)^*$ excited state, demonstrating the energetic possibility of proton transfer from the **E** to **K** form in excited state.

The excited state conversion from the **E** to the **K** structure is a complex process that intimately links electronic and structural reorganization. It is interesting to follow in a first step the geometric changes of **E** in the ground and in the lowest $^1(\pi\pi)$ excited state. The experimental data suggested a dramatic lowering of the pK_a values of 7H4MC when moving from the ground to the excited state (S_0 (∼7.7) to S_1 (0.45)).[32] The gas phase calculations of the **E** form showed insignificant increase of O−H bond length (by 0.001 Å) in the excited state. The $\pi\pi^*$ excited states of enol-$(H_2O)_2$ and enol-$(H_2O)_4$ clusters, where part of the first solvation shell is included, indicated larger O−H elongation, with 0.006 and 0.007 Å (Figure 4). The result thus obtained is in agreement with increasing acidity of the **E** form in excited state. Deprotonation energies (DE) and proton affinities (PA) (calculated as enthalpy and Gibbs energy

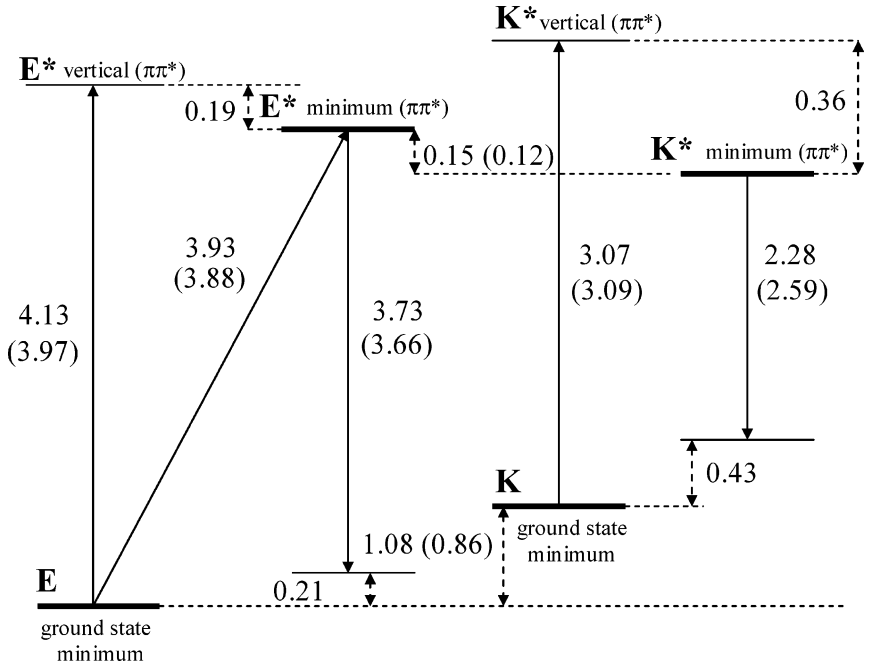

Figure 5. Energy diagram for the proton transfer in 7H4MC. Excitation and fluorescence scheme and transition energies (in eV) for the **E** and **K** forms; the transition energies in aqueous solution are given in parentheses.

TABLE 6: Relative Energies, (Δ*E*), Enthalpies (Δ*H*) and Gibbs Free Energies (Δ*G*), in kcal/mol, of the E and K Forms of 7H4MC in the Gas Phase and in Aqueous Solution (PCM) at the B3LYP/SVPD Level

species[a]	gr st gas	gr st[a] aq sol	$^1\pi\pi^*$ [b] gas	$^1\pi\pi^*$ [b] aq sol	$^1\pi\pi^*$ [c] gas	$^1\pi\pi^*$ [c] aq sol
enol (**E**)	0.0	0.0	0.0	0.0	0.0	0.0
keto (**K**)						
Δ*E*	24.83	19.75	0.35	−0.63	−3.49	−2.68
ΔH_{298}	24.55	19.46			−2.45	−1.64
ΔG_{298}	23.79	18.71			−2.02	−1.21
enol-$(H_2O)_2$	0.0	0.0	0.0	0.0	0.0	0.0
Δ*E*(keto-$(H_2O)_2$)	20.31	15.91	−1.63	−1.72	−5.53	−3.09
enol-$(H_2O)_4$	0.0	0.0	0.0	0.0	0.0	0.0
Δ*E*(keto-$(H_2O)_4$)	17.23		−4.22		−8.12	−2.77

[a] PCM energy of optimized ground state structure in aqueous solution. [b] Franck−Condon excited state structures. [c] Stationary excited state structures.

TABLE 7: Deprotonation Energies[a] (DE) and Proton Affinities[a] (PA), in kcal/mol, of the E and K Forms of 7H4MC at the B3LYP/SVPD Level

species	gr st gas phase	gr st[b] aq sol	$\pi\pi^*$ [c] gas phase	$\pi\pi^*$ [c] aq sol
	Deprotonation Energies			
E	326.8 (327.0)[d]	287.6 (291.0)	307.8	280.5
K	302.3 (303.2)	268.1 (268.1)	310.3	276.9
	Proton Affinities			
E	216.6 (216.8)	260.9 (257.9)	228.6	268.4
K	241.1 (241.0)	280.4 (280.0)	226.1	266.8

[a] Including enthalpy correction. [b] PCM energy of optimized ground state structure in solution. [c] Stationary excited state structures. [d] Gibbs energies are given in parentheses.

differences) in the ground and the excited state of **E** and **K**, both in the gas phase and in solution are presented in Table 7. It is found that (i) DE for the **E** form in the ground and in the $^1(\pi\pi^*)$ excited states decreases by 39 and 28 kcal/mol, respectively, when going to the aqueous solution and (ii) in the gas phase and in solution DE decreases for **E** when going from the ground to the excited state. At the same time, the proton affinity calculations for the **E** form showed that (i) in solution the PA of the ground and the excited states increase and (ii) PA is larger in the excited state than in the ground state (considering both gas phase and solution).

IV. Conclusions

TDDFT in combination with the SVPD basis set is a computationally efficient method reliable enough to describe the excitation and fluorescence properties of coumarins with sufficient accuracy. The TDDFT results were confirmed with RI-CC2 calculations. The gas phase calculations gave as the lowest singlet excited state for the **E** and **C** forms a $^1A'(\pi\pi^*)$ state and for the **K** and **A** forms a $^1A''$ state, $n\pi^*$ and $\pi\sigma^*$, respectively. This finding corrects previous semiempirical results for the **E** form where a reversed state ordering had been found. The calculated fluorescence energies in the gas phase revealed a $\pi\pi^*$ character of the lowest emitting state for **A** and **C** and $n\pi^*$ character for **E** and **K.** The 7H4MC−solvent (water) effects on the lowest excited states was computed using a continuum approach (PCM) simulating bulk solvent interactions, 7H4MC−water clusters, simulating specific solvent interactions and a combination of both methods by embedding the cluster in a continuum. It was found that the PCM model reproduces well the solvent interaction and estimates quite reliably the solvent shift of singlet excitation and fluorescence energies of the species studied. The calculations in aqueous solution revealed that $^1(\pi\pi^*)$ state is the lowest state for excitation and fluorescence transitions for both neutral and ionic species of 7H4MC. The calculated vertical excitation and fluorescence energies in aqueous solution are in good agreement with experiment. The calculations showed that depending on the polarity of the medium the solvent shifts vary such that a change in the character of the lowest excited and fluorescing state occurs. This finding is in full agreement with experiment. Correlation between the calculated dipole moment of the excited state and the solvent shift was found. With an increase of the dipole

moment of the excited state (relative to the ground state) the solvent shift is negative, lowering the transition energy and *vice versa*.

In solution, the **K** structure of the $^1\pi\pi^*$ state is of lower energy than the **E** structure. This finding confirms the energetic possibility of proton transfer from the **E** to the **K** form in the excited state. The calculated structural parameters and thermodynamic characteristics of the **E** showed that in the $^1\pi\pi^*$ state the O−H deprotonation energy decreases and the proton affinity of the carbonyl oxygen increases. In conclusion, the results obtained in our theoretical study assist the interpretation of the spectroscopic data, refine explicitly ambiguous discussions in the literature and provide a better understanding of the complex photophysical and photochemical behavior of 7-hydroxy-4-methylcoumarin.

Acknowledgment. I.G. acknowledges financial support by the Austrian Academy of Sciences during her stay at the Institute for Theoretical Chemistry, University of Vienna, in the framework of the Bilateral Exchange Agreement Austria-Bulgaria. We thank Professor Peter Schuster for his support of this work. We acknowledge also support by the Austrian Science Fund within the framework of the Special Research Program F16 and Project P14817-N03. The calculations were performed in part on the Schrödinger II cluster of the University of Vienna.

Supporting Information Available: Total energies and Cartesian geometries for the stationary points investigated; Expanded Figure 3a−c of HOMO and LUMO for **K**, **C**, and **A** forms, respectively; Expanded Table 5. This material is available free of charge via the Internet at http://pubs.acs.org.

References and Notes

(1) Drexhage, K. H. In Dye-Lasers. *Topics in Applied Physics*, 2nd ed.; Schäfer, F. P., Ed.; Springer-Verlag: New York, 1990.
(2) McCarthy, P. K.; Blanchard, G. J. *J. Phys. Chem.* **1993**, *97*, 12205.
(3) Moylan, C. R. *J. Phys. Chem.* **1994**, *98*, 13513.
(4) Jones, G., II; Jimenez, J. A. C. *J. Photochem. Photobiol. B* **2001**, *65*, 5.
(5) Bangar Raju, B.; Costa, S. M. B. *J. Phys. Chem. B* **1999**, *103*, 4309.
(6) (a) Kaholek, M.; Hrdovie, P. *J. Photochem. Photobiol. A* **1997**, *108*, 283. (b) Fletcher, A. N.; Bliss, D. *Appl. Phys*. **1986**, *16*, 289. (c) Wolfbeis, O. S.; Furlinger, E.; Kroneis, H.; Marsoner, H. *Z. Anal. Chem.* **1983**, *314*, 577.
(7) Moriya, T. *Bull, Chem. Soc. Jpn* **1986**, *59*, 961.
(8) Kumar, S.; Giri, R.; Machwe, M. K. *Ind. J. Pure Appl. Phys*. **1998**, *36*, 622.
(9) Nielsen, B. E. Coumarins patterns in the Umbrelliferae. In *The Biology and Chemistry of the Umbrelliferae*; Heywood, V. H., Ed.; Academic Press: London, 1971; p 325.
(10) Ammar, H. O.; Ghorab, M.;. Nahhal, S. A.; Makram, T. S. *Pharmazie* **1997**, *52*, 946.
(11) Kam, C. M.; Kerrigan, J. E.; Plaskon, R. R.; Duffy, E. J.; Lollar, P.; Suddath, F. L.; Powers, J. C. *J. Med. Chem.* **1994**, *37*, 1298.
(12) Yamada, Y.; Okamoto, M.; Kikuzaki, H.; Nakatani, N. *Biosci., Biotechnol., Biochem.* **1997**, *61*, 740.
(13) Rosskopt, F.; Kraus, J.; Franz, G. *Pharmazie* **1992**, *47*, 139.
(14) McCulloch, P.; George, W. D. *Br. J. Cancer* **1989**, *59*, 179.
(15) Lazarova, G.; Kostova, I.; Neychev, H. *Fitoterapia* **1993**, *64*, 134.
(16) Matolcsy, G.; Nadasy, M.; Andriska, V. *Pesticide Chemistry*; Studies in Environmental Science, Vol. 32; Elsevier: Budapest, 1988.
(17) Pavlopoulos, T. G. *IEEE J. Quantum Elec.* **1973**, *9* (5), 510.
(18) Zinsli, P. E. *J. Photochem*, **1974/75**, *3*, 55.
(19) Schulman, S. G.; Rosenberg, L. *J. Phys. Chem.* **1979**, *83*, 3 (4), 447.
(20) Moriya, T. *Bull. Chem. Soc. Jpn.* **1983**, *56*, 6.
(21) Moriya, T. *Bull. Chem. Soc. Jpn.* **1988**, *61*, 1873.
(22) Bardez, E.; Boutin, P.; Valeur, B. *Chem. Phys. Lett.* **1992**, *191*, 142.
(23) Abu-Eittan, R. H; El-Tawil, B. A. H. *Can. J. Chem.* **1985**, *63*, 1173.
(24) Traven, V. F.; Vorobjeva, L. I.;. Chibisova, T. A.; Carberry, E. A.; Beyer, N. J. *Can. J. Chem*. **1997**, *75*, 365.
(25) Seixas de Melo, J.; Fernandes, P. F. *J. Mol. Struct.* **2001**, *565*−*566*, 69.
(26) Hoshiyama, M.; Kubo, K.; Igarashi, T.; Sakurai, T. *J. Photochem. Photobiol.* **2001**, *138*, 227.
(27) Novak, I.; Kovac, B. *J. Elec. Spectrosc. Relat. Phenom.* **2000**, *113*, 9.
(28) Kovac, B., Novak, I. *Spectrochim. Acta A* **2002**, *58*, 1483.
(29) Seixas de Melo, J.; Macanita, A. L. *Chem. Phys. Lett.* **1993**, *204*, 556.
(30) Chou, Pi-Tai; Martinez, M. L.; Styder, S. L. *Chem. Phys. Lett.* **1992**, *188*, 49.
(31) Seixas de Melo, J. S.; Becker, R. S.; Macanita, A. L. *J. Phys. Chem.* **1994**, *98*, 6054.
(32) Mikes, V. *Collection Czech. Chem. Commun.* **1979**, *44*, 508.
(33) Cave, R. J.; Burke, K.; Castner, E. W., Jr. *J. Phys. Chem. A* **2002**, *106*, 9294.
(34) Sobolewsi A. L.; Domcke, W. *Phys. Chem. Chem. Phys.* **1999**, *1*, 3065.
(35) Aquino, A. J. A.; Lischka H.; Hättig, Ch. *J. Phys. Chem. A*, **2005**, *109*, 3201.
(36) Furche, F.; Ahlrichs, R. *J. Chem. Phys.* **2002**, *117*, 7433.
(37) Georgieva, I.; Mihaylov, T.; Bauer, G.; Trendafilova, N. *Chem. Phys.* **2004**, *300*, 119.
(38) Christiansen, O.; Koch, H.; Jørgensen, P. *Chem. Phys. Lett*, **1995**, *243*, 409.
(39) Hättig, C. *J. Chem. Phys.* **2003**, *118*, 7751.
(40) Köhn, A.; Hättig, C. *J. Chem. Phys.* **2003**, *119*, 5021.
(41) Tomasi, M. Persico *Chem. Rev.* **1994**, *94*, 2027.
(42) Cramer, C. J.; Truhlar, D. J. *Chem. Rev.* **1999**, *99*, 2161.
(43) Ahlrichs, R.; Bär, M.; Häser, M.; Horn, H.; Kölmel, C. *Chem. Phys. Lett.* **1989**, *162*, 165.
(44) Bauernschmitt, R.; Ahlrichs, R. *Chem. Phys. Lett.* **1996**, *256*, 454.
(45) Bauernschmitt, R.; Häser, M.; Treutler, O.; Ahlrichs, R. *Chem. Phys. Lett.* **1997**, *264*, 573.
(46) Becke, A. D. *J. Chem. Phys*. **1993**, *98*, 5648.
(47) Schäfer, A.; Horn, H., Ahlrichs, R. *J. Chem. Phys.* **1992**, *97*, 2571.
(48) Schäfer, A.; Huber, C.; Ahlrichs, R. *J. Chem. Phys.* **1994**, *100*, 5829.
(49) Weigend, F.; Häser, M.; Patzelt, H.; Ahlrich, R. *Chem. Phys. Lett.* **1998**, *294*, 143.
(50) Miertuš, S.; Scrocco, E.; Tomasi, J. *Chem. Phys.* **1981**, *55*, 117.
(51) Miertuš, S.; Tomasi, J. *Chem. Phys.* **1982**, *65*, 239.
(52) Cossi, M.; Barone, V.; Cammi, R.; Tomasi, J. *Chem. Phys. Lett.* **1996**, *255*, 327.
(53) Frisch, M. J.; Trucks, G. W.; Schlegel, H. B.; Scuseria, G. E.; Robb, M. A.; Cheeseman, J. R.; Montgomery, J. A., Jr.; Vreven, T.; Kudin, K. N.; Burant, J. C.; Millam, J. M.; Iyengar, S. S.; Tomasi, J.; Barone, V.; Mennucci, B.; Cossi, M.; Scalmani, G.; Rega, N.; Petersson, G. A.; Nakatsuji, H.; Hada, M.; Ehara, M.; Toyota, K.; Fukuda, R.; Hasegawa, J.; Ishida, M.; Nakajima, T.; Honda, Y.; Kitao, O.; Nakai, H.; Klene, M.; Li, X.; Knox, J. E.; Hratchian, H. P.; Cross, J. B.; Bakken, V.; Adamo, C.; Jaramillo, J.; Gomperts, R.; Stratmann, R. E.; Yazyev, O.; Austin, A. J.; Cammi, R.; Pomelli, C.; Ochterski, J. W.; Ayala, P. Y.; Morokuma, K.; Voth, G. A.; Salvador, P.; Dannenberg, J. J.; Zakrzewski, V. G.; Dapprich, S.; Daniels, A. D.; Strain, M. C.; Farkas, O.; Malick, D. K.; Rabuck, A. D.; Raghavachari, K.; Foresman, J. B.; Ortiz, J. V.; Cui, Q.; Baboul, A. G.; Clifford, S.; Cioslowski, J.; Stefanov, B. B.; Liu, G.; Liashenko, A.; Piskorz, P.; Komaromi, I.; Martin, R. L.; Fox, D. J.; Keith, T.; Al-Laham, M. A.; Peng, C. Y.; Nanayakkara, A.; Challacombe, M.; Gill, P. M. W.; Johnson, B.; Chen, W.; Wong, M. W.; Gonzalez, C.; Pople, J. A. *Gaussian 03*, revision C.02; Gaussian, Inc.: Wallingford, CT, 2004.
(54) Cossi, M.; Rega, N.; Scalmani, G.; Barone, V. *J. Chem. Phys.* **2002**, *117*, 43.
(55) Brandsen, B. H.; Joachain, C. J. *Physics of Atoms and Molecules*, Longman Group Limited: London; New York, 1983.
(56) Antol, I.; Eckert-Maksiæ, M.; Müller, Th.; Dallos, M.; Lischka, H. *Chem. Phys. Lett.* **2003**, *374*, 587.
(57) Andrade do Monte, S.; Müller, Th.; Dallos, M.; Lischka, H.; Diedenhofen, M.; Klamt, A. *Theor. Chem. Acc*. **2004**, *111*, 78
(58) Agmon, N. *J. Chem. Phys.* **1990**, *94*, 2959.